Pittsburgh MR Imaging Community Retreat

University of Pittsburgh Biomedical Science Tower

November 5, 2015

11:30 am to 5:00 pm

Sponsored by
University of Pittsburgh School of Medicine, Department of Radiology,
and the Magnetic Resonance Research Center

Pittsburgh MR Imaging Community Retreat

University of Pittsburgh Biomedical Science Tower

November 5, 2015

11:00-11:30 **Poster set up and registration** (BST lobby)

11:30-11:40 **Introduction** (BST S120)
Hoby Hetherington, PhD: Professor of Radiology and Director of the MRRC
Moira Hitchens, PhD: Scientific Administrator of Radiology

11:45-1:15 **Poster Session and Lunch** (BST lobby)

Talks (BST120)

1:15-1:40 T. Kevin Hitchens, PhD, MBA: Animal Imaging Center, University of Pittsburgh: ***"Small Animal Imaging at the University of Pittsburgh"***

1:45-2:10 Ashok Panigrahy, MD: Pediatric Imaging Research Center at Children's Hospital of Pittsburgh: "***New Developments in Advanced Pediatric Imaging***"

2:15-2:40 Ying Yang, PhD: Scientific Imaging and Brain Research Center, CMU:
"*Two examples of multimodal imaging convergence at SIBR: Simultaneous EEG and fMRI to decode semantics and Diffusion-weighted imaging and fcMRI to detect structural and functional changes following spatial learning*"

2:40-2:55 Coffee Break

2:55-3:20 Michael Dickey, PhD: Neuroscience Imaging Center (NIC), University of Pittsburgh:
"*Lesion-deficit analyses in aphasia: Current research at the Neuroscience Imaging Center (NIC)*"

3:25-3:50 Yijen Wu, PhD: Animal Imaging Core, Rangos Research Center at Children's Hospital of Pittsburgh: **"*The Good, the Bad, and the Ugly*"**

3:55-4:20 Hoby Hetherington, PhD: Magnetic Resonance Research Center, University of Pittsburgh: "***New methods and opportunities at the MRRC***"

4:20-4:35 Hoby Hetherington: Poster Award Presentation and Closing Remarks

4:40-4:55 Poster Removal

POSTERS

MR and Preclinical Models

MR Acquisition, Analysis, and Hardware

Imaging of the CNS

In Vivo Metabolic and Structural Imaging at 7T after Mild Traumatic Brain Injury in Immature Rats

Emin Fidan[1], Lesley Foley[2], Lee Ann New[1], Patrick M Kochanek[1], T. Kevin Hitchens[2,3], Hülya Bayır[1].

[1]Safar Center for Resuscitation Research, University of Pittsburgh. [2]Pittsburgh NMR Center for Biomedical Research, Carnegie Mellon University. [3]Animal Imaging Center, University of Pittsburgh, PA.

Inroduction: Mild traumatic brain injury(mTBI) in children is a common and serious public health problem. Conventional neuroimaging findings are often normal in children who sustain mTBI putting them at risk for repeated mTBI (rmTBI). There is a need for more sensitive imaging techniques capable of detecting subtle alterations in neurophysiology after injury. In a pre-clinical model, we examined neurochemical and white matter changes in immature brain resulting from mTBI and rmTBI using proton magnetic resonance spectroscopy (MRS) and diffusion tensor imaging (DTI).

Methods: Eighteen day old male rats received Sham, mTBI, or rmTBI (three impacts 24h apart). MRS of the hippocampi and in vivo DTI of whole brain were examined at 7 Tesla 7 days after injury after which rats were sacrificed for immunohistochemical staining (Silver and APP).

Results: After mTBI and rmTBI, N-acetylaspartate/creatine ratio (NAA/Cr) was reduced (p=0.03, p<0.0001, respectively), and the myo-inositol/creatine ratio (Ins/Cr) increased (p=0.017, p=001, respectively) vs sham. rmTBI exacerbated the reduction in NAA/Cr (p=0.01 vs mTBI). The choline/creatine (Cho/Cr) and lipid/creatine (Lip/Cr) ratios were also decreased (p=0.04, p=0.02, respectively) after rmTBI vs sham. There were significant increases in axial diffusivity, radial diffusivity and significant decreases in fractional anisotropy primarily in ipsilateral corpus callosum, external capsule, hippocampus and cortex after rmTBI vs sham. Immunohistochemistry revealed argyrophilic axonal staining and APP positive axonal bulbs in external capsule at 7d post mTBI and rmTBI.

Conclusion: NAA and Ins are altered after mTBI and rmTBI likely reflecting neuro-axonal cell damage and glial proliferation, respectively. The decrease in Cho and Lip after rmTBI, DTI and histological findings may reflect damage to axonal membrane. These findings may be relevant to understanding the extent of disability following mTBI and rmTBI in the immature brain.

Support: NS061817, NS076511.

Study of Systemic Inflammation Following Blast Exposure using ^{19}F MRI Cell Tracking

Lesley M. Foley[1], Cory A. Riccio[2], James C. DeMar[2], Patrick M. Kochanek[3,4], Joseph B. Long[2], T. Kevin Hitchens[1,5]

[1]Pittsburgh NMR Center for Biomedical Research, Carnegie Mellon University, Pittsburgh, PA, [2]Center for Military Psychiatry and Neuroscience, Walter Reed Army Institute of Research, Silver Spring, MD, [3]Safar Center for Resuscitation Research, University of Pittsburgh School of Medicine, Pittsburgh, PA, [4]Departments of Critical Care Medicine, Pediatrics and Anesthesiology, University of Pittsburgh School of Medicine, Pittsburgh, PA, [5]Animal Imaging Center, University of Pittsburgh, Pittsburgh PA.

BACKGROUND AND SIGNIFICANCE

Blast injury results in multiple organ damage and overpressure alone may not precisely indicate the level of injury after blast exposure. Therefore assessment of the extent of injury to the body following blast exposure is important. The purpose of this study was to examine systemic inflammation by MRI following blast exposure by tracking macrophage/monocyte infiltration by the labeling of these cells with a fluorine contrast agent.

METHODS

Rats (n=19) were anesthetized and exposed to a single or repeated blast overpressure (19.2 psi); a group of sham rats did not undergo blast. At different time points rats were injected with a fluorine contrast agent (VS580, Cellsense, Pittsburgh, PA), euthanized and fixed.

The rats were imaged in 4 sections, on a 7T 21 cm Bruker Biospec AVANCE 3 scanner. ^{19}F quantification was performed over 128 slices in each rat using Voxel Tracker software.

RESULTS

82 regions of interest were identified that contained fluorine-labeled macrophages throughout the bodies of the animals in all groups. The injury itself is very heterogeneous, but one obvious result was that suffering a second blast one minute after the first increased the amount of fluorine signal seen in these animals, which most likely represents increased macrophage accumulation.

CONCLUSION

These findings demonstrate that ^{19}F MRI is effective in detecting systemic injury as a result of shock tube-generated overpressure. More work needs to be done to explore the role that systemic inflammation has on acute and chronic injury, following blast.

Modification of Nanoemulsions with ^{19}F MRI Imaging Capabilities to Incorporate PET Imaging Modalities

Michele Herneisey,[1] Marie Caline Abadjian,[2] Wissam Beaino,[2] Sravan Kumar Patel,[1] Carolyn J. Anderson,[2] Jelena M. Janjic*[1]

[1] Graduate School of Pharmaceutical Science, Mylan School of Pharmacy, Duquesne University, Pittsburgh PA, US
[2] University of Pittsburgh, Department of Radiology, Pittsburgh PA, US

Magnetic resonance (MR) imaging is a valuable imaging technique, as it is capable of capturing high resolution anatomic information with excellent soft-tissue contrast. Positron emission tomography (PET) lacks the resolution possible through MRI, but has a significant advantage in that it is the only imaging technique capable of tracking radiolabeled biomarkers *in vivo* with a detection sensitivity near the picomolar range. Thus, the combination of MRI and PET imaging modalities into a single system could prove extremely advantageous. PET-MRI has advantages over other combination imaging systems, such as PET-CT, including the fact that PET and MRI preserve their functionality when operated isochronously,[1] and the decreased radiation burden to patients. Our group recently developed a theranostic perfluorocarbon nanoemulsion platform for targeted delivery of a cyclooxygenase-2 (COX-2) inhibitor (celecoxib) to macrophages.[2-5] These nanoemulsions contain both ^{19}F MRI and NIR imaging modalities. We propose to improve this platform through the addition of a ^{64}Cu chelator, thus enabling nanoemulsion visualization via three modalities (NIR/MRI/PET). Our group has effectively conjugated a hydrophilic copper chelator to a lipid chain, creating in effect, a surfactant. Here, we demonstrate the successful incorporation of this chelator-lipid compound into a nanoemulsion using a combination of thin film and microfluidization techniques. Formulation strategy (thin film followed by microfluidization) did not affect nanoemulsion properties. The developed nanoemulsion maintains colloidal stability over a period of three months and when exposed to stress from centrifugation and cell culture conditions. Preliminary data presented here shows progress towards radiolabeling of nanoemulsions with ^{64}Cu.

Chemical exchange-sensitive spin-lock MRI of glucose and deoxyglucose in brain tumors

[1]Tao Jin, [1]Bistra Iordanova, [1]Ping Wang, [2]Seong-Gi Kim

[1]Department of Radiology, University of Pittsburgh, Pittsburgh, Pennsylvania
[2]Center for Neuroscience Imaging Research, Institute for Basic Science; Department of Biomedical Engineering, Sungkyunkwan University, Suwon, Korea

Background: Recent chemical exchange saturation transfer (CEST) MRI studies with administration of non-labelled D-glucose (Glc) and 2-deoxy-D-glucose (2DG) had demonstrated the capability of tumor detection.

Significance: We evaluated the efficacy of an alternative method, glucoCESL, for the study of brain tumor, which presumably has better sensitivity than the CEST technique.

Methods: Brain MR images of Fisher rats bearing 9L glioma were acquired. A time series of spin-lattice relaxation rate in the rotating frame ($R_1\rho$) were measured with an intravenous injection of 1 g/kg Glc (n = 4) or 0.25 g/kg of 2DG (n = 3). T_1-weighted EPI images were acquired before and after an injection of Gd-DTPA to delineate the tumor region.

Results: Fig. 1A shows the Gd-enhanced images, in which the glioma can be identified as the hyperintense region. Fig. 1B and 1C show the relative $R_1\rho$ change maps of CESL with injection of Glc and 2DG, respectively. Fig. 2 shows the averaged time courses of the $R_1\rho$ change induced by Glc and 2DG injections obtained from an ROI of normal contralateral tissue versus that from the tumor region. For both Glc and 2DG, the faster onset-to-peak time and larger magnitude of $R_1\rho$ response for tumor may be attributed to an elevated cellular glucose uptake, and/or an impaired blood brain barrier in the tumor vasculature. The difference between Glc- and 2DG-CESL results may indicate their different metabolic properties.

Conclusion: Our results indicate that glucoCESL has high sensitivity and can be applied for the diagnosis and prognosis of brain tumor.

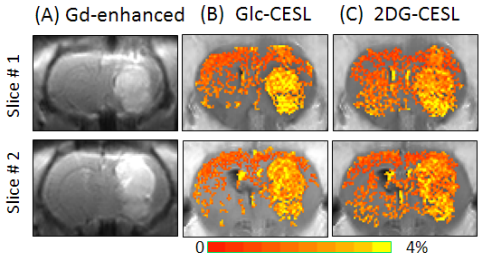

Fig. 1

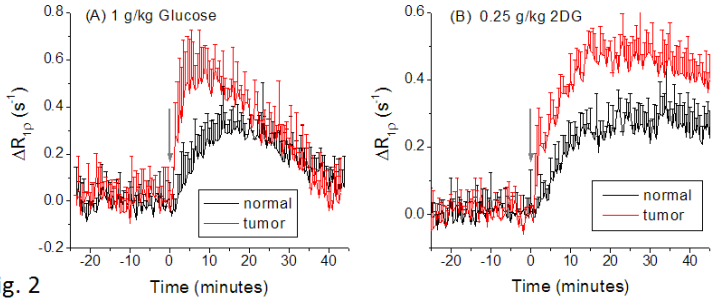

Fig. 2

Process development for large scale production of theranostic nanoemulsions

Lu Liu[1], Christina Bagia[1], Jelena Janjic[1,2]

[1]Graduate School of Pharmaceutical Sciences, Duquesne University, Pittsburgh, Pennsylvania, United States
[2]McGowan Research Institute for Regenerative Medicine, Pittsburgh, Pennsylvania, United States

Theranostic nanomedicines show great potential as future personalized medicines. Though much progress has been made in their preclinical applications, their clinical utilization is still under development. One of key ingredients for successful theranostic nanomedicine translation is pharmaceutical process design for their production in scale. In a recent study (Liu et al, Bioresearch Open 2015) we reported a successful scale up of a model theranostic nanomedicine – anti-inflammatory drug loaded multimodal imaging (NIR/19F MRI) nanoemulsion. Celecoxib was loaded into near-infrared labeled perfluorocarbon nanoemulsion and produced on three scale levels (small at 54 mL, medium at 270 mL and large at 1000 mL) by combination of sonification and microfluidization. Drug content in the largest scale nanoemulsion is 96.9% as tested by HPLC. The average size and polydispersity were not affected by equipment used (M-110EH-30 for medium and large scale, M110S for small scale) or production scale. The overall nanoemulsion stability was also maintained upon scale up. The average droplet size was 150 nm, and the average zeta potential was -7 mV. During the course of this study we have developed quality assessment protocols. We evaluated the nanoemulsions for particle size, drug loading, and colloidal stability in all three scales up to 300 days. Nanoemulsions were stable under elevated temperature 37^{o}C in different modeled biological conditions. The stress such as centrifugation and filtration did not affect the particle size either. We also tested toxicity, and pharmacological effect of nanoemulsions in RAW 264.7 macrophages. All nanoemulsions produced showed no toxic effects on cells upon prolonged exposure. PGE_2 ELISA assay confirmed that large-scale nanoemulsions retained its anti-inflammatory properties in macrophages. The study presented here builds upon these results. First, we will increase the celecoxib loading by modifying the surfactant/oil ratio. Second, we will test the effects of perfluorocarbons on scale up and drug incorporation. Third, the scale up effect on near-infrared dyes in the nanoemulsions is also tested. Taken together, this study further expands our understanding of the scale up and process design impact on overall theranostic nanoemulsion quality.

This poster has been presented at the ACS colloids conference in Summer 2015.

Pharmacological blockade of inhibitory neuronal activation reduces the evoked fMRI response to LOT stimulation in the rat olfactory bulb

Alexander John Poplawsky[1], Hiro Fukuda[1], and Seong-Gi Kim[2]

Radiology, University of Pittsburgh, Pittsburgh, PA, USA[1]; Biomedical Engineering, Center for Neuroscience Imaging Research, Institute for Basic Science (IBS), SKKU,

Suwon, Korea[2]

Background and Significance: It is currently unknown if the evoked activities of inhibitory neurons contribute to the fMRI response. In the olfactory bulb, inhibitory neurons are almost exclusively targeted by stimulation of the lateral olfactory tract (LOT). We previously showed that fMRI signals increase due to LOT stimulation; but it is unknown whether this vascular response is initiated by the presynaptic glutamate release (e.g. through astrocyte detection) or by postsynaptic inhibitory neuronal coupling.

Methods: In isoflurane-anesthetized rats, LOT was continuously stimulated in a block design experiment; and cerebral blood volume-weighted fMRI responses were measured at 9.4 T. Next, to decrease the evoked activity of inhibitory neurons, 25-mM APV (NMDA receptor antagonist) was applied to the dorsal surface of the bulb during fMRI: 60-min vehicle (baseline), 90-min APV (drug), and 180-min vehicle washout (recovery) periods.

Results: Evoked fMRI signal change maps were correlated to the drug delivery paradigm. Significant drug effects ($p < 0.01$) penetrated only ~1-2 mm below the drug application site. Here, the average evoked signal change for LOT stimulation was 4.9 ± 1.0% (mean ± SEM, n = 5 rats) for the baseline, 1.5 ± 0.7% for the drug ($p = 0.007$, paired T-test, baseline vs. drug), and 4.3 ± 0.7% for the recovery periods. The evoked fMRI signal decreased by 72.9 ± 12.7% relative to baseline during the drug period compared to 6.1 ± 15.5% during the recovery period ($p = 0.005$, paired T-test).

Conclusions: Postsynaptic activities of inhibitory granule cells contribute to the evoked fMRI response.

Neuronal and Physiological Correlation of Hemodynamic Resting-State Fluctuations and Connectivity

Alberto Vazquez[1], Matthew Murphy[1], Seong-Gi Kim[2]

1University of Pittsburgh, Pittsburgh, PA, 2Sunkyunkwan University, Suwon, Korea, Republic of

Introduction:

Low-frequency, spatially coherent fluctuations present in functional magnetic resonance imaging (fMRI) time series have had a tremendous impact on brain connectomics. To properly interpret these hemodynamic connectivity measures, studies have been performed to investigate the relationship between these fluctuations and neural activity [1-5]. However, fundamental gaps remain regarding the relationship between these fluctuations and neuronal activity due to the complex and vascular nature of the fMRI signal. Studies in rodents have shown the presence of these hemodynamic fluctuations using fMRI and analogous optical methods under awake and lightly anesthetized conditions [6-8]. This work used an ideally positioned and unique animal model to investigate the degree with which hemodynamic connectivity is associated with neuronal, metabolic, and vascular connectivity measures.

Methods:

Transgenic mice expressing GCaMP3, a fluorescent calcium indicator that reports changes in intracellular calcium concentration that accompany spiking activity [10], were used to simultaneously image low-frequency changes in neuronal activity (GCAMP) as well as hemodynamic measurements of blood oxygenation (OIS-BOLD, analogous to fMRI) and cerebral blood volume (OIS-CBV, to assess purely vascular contributions) from the same animals (n=7). Nontransgenic mice (n=4) were used to simultaneously image oxidative metabolism activity using flavoprotein autofluorescence imaging (FAI [10]) along with hemodynamic measurements of blood oxygenation and blood volume. Bihemispheric
GCAMP, FAI, OIS-BOLD and OIS-CBV images were acquired at 10 Hz from the exposed superior surface of the mouse brain under light ketamine anesthesia (30 mg/kg/hr) for 5 to 20 min periods. The analysis consisted of temporal band-pass filtering (0.02-0.20Hz) and k-means clustering over one hemisphere (Figure 1). Then, overlap coefficient, connectivity correlation and spatial correlation matrices were generated and compared across modalities.

Results:

Although network clusters calculated using either GCaMP (neuronal activity) or hemodynamic data (OIS-BOLD, OIS-CBV) did not exhibit strong overlap fraction (r=0.334 +/- 0.07 s.d. for GCAMP vs. OIS-BOLD and r=0.333 +/- 0.08 s.d. for GCAMP vs. OIS-CBV), the strength of the correlation of inter-cluster connectivity matrix elements between imaging modalities were strongly correlated with one another (r=0.780 +/- 0.11 s.d. for GCAMP vs OIS-BOLD and r=0.577 +/- 0.23 for GCAMP vs. OIS-CBV) (Figure 2). This finding suggests that hemodynamic connectivity as measured by blood oxygenation measurements is a valuable surrogate of the underlying neuronal connectivity. In nontransgenic animals, greater correlation of the inter-cluster connectivity was observed between tissue oxidative metabolism (FAI) and blood oxygenation measurements, suggesting that metabolic contributions to hemodynamic signals are likely responsible for its significant correlation with neuronal connectivity (average r=0.617 for FAI vs. OIS-BOLD compared to average r=0.441 for FAI vs. OIS-CBV).

Conclusions:

Therefore, these findings suggest that metabolism-sensitive measurements similar to those used in this work (e.g. BOLD fMRI, OIS-BOLD and FAI) are well positioned to capture changes in neuronal connectivity compared to purely vascular measurements (e.g. OIS-CBV, ASL fMRI).

RF Shimming Approaches for 7T Multi-row Transceiver Arrays

HP Hetherington[1], T Zhao[2], PM Starewicz[3] and JW Pan[1],
University of Pittsburgh, Siemens Medical Systems and Resonance Research Inc.

Introduction: Achieving adequate B_1 amplitude, homogeneity and coverage are critical components for imaging and MRSI at 7T. Previously we demonstrated that RF shimming with an 8-element transceiver array enables peak B_1 amplitudes of 23.4uT (1.0 kHz) at moderate peak total powers (2-4kW) and RF shimming based outer volume suppression (OVS) for MRSI. To maintain high efficiency for reception and transmission, relatively small coils (7- 10cm in length) are used which limit brain coverage for single row coils. To expand coverage to the entire brain we developed an 8x2 (8 elements per row x 2 row) transceiver array. To drive the coil efficiently with only 8 independent transmit channels, splitters or RF multiplexing must be used. In this work describe two configurations for RF splitting which provide high homogeneity and support RF shimming based (OVS) for MRSI.

Methods: All data were acquired on an 8 channel parallel transmit 7T Siemens human MRI system using an 8x2 transceiver array and a higher order shim insert (Resonance Research Inc.). Using 8 independent RF channels the 16 coil transceiver array was driven in two configurations: A - which uses 4 independent drives for each row of coils accommodating the smaller size and higher efficiency of the superior row, and B – which maximizes in-plane phase adjustment flexibility and enables RF shimming based outer volume suppression (Fig 1). Anatomical images were acquired with an MP2RAGE sequence using GRAPPA 3 and 0.7mm isotropic resolution. MRSI data was acquired using a J-refocused MRSI sequence, using 1st-4th degree shimming.

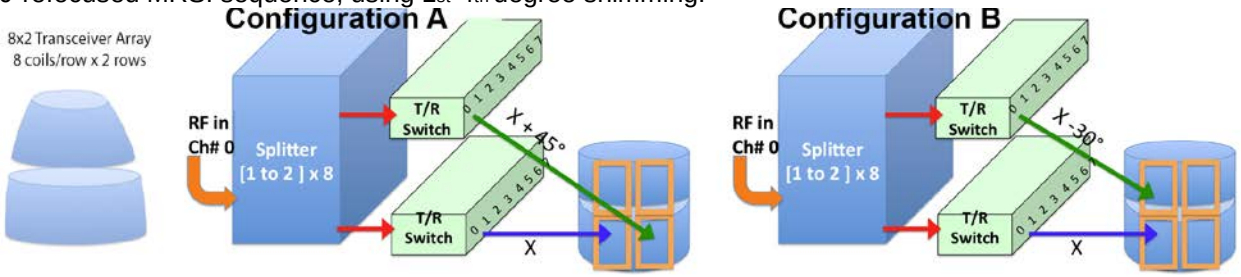

Results: Displayed in Fig. 2A,B are orthogonal slices from a 3D MP2RAGE image demonstrating the extent of coverage for the 8x2 array in both configurations. A B_1 amplitude of 17.6μT (750Hz) was reached in both configurations for all subjects with all RF drive voltages below 150V and most below 120V. Fig. 2D,E display B_1 maps for the homogeneous distribution for both configurations using a single set of amplitudes and phases for all slices. Although configuration A achieves superior homogeneity over the entire brain within the slice (Fig 2C - SD=10.4±1.8%, n=8 subjects) configuration B also achieves good homogeneity (SD=11.8±3.1%, n=10 subjects). For configuration B, the use of a single drive voltage for coils in different rows results in gradient of increasing RF amplitude along the Z-axis. Displayed in Fig 2F are B_1 maps for configuration B showing the ring distribution used for MRSI OVS. This provides simultaneous OVS throughout the entire brain. Displayed in Fig 3 are MRSI data acquired from the cingulate and hippocampus using identical RF shimming values for both slices.

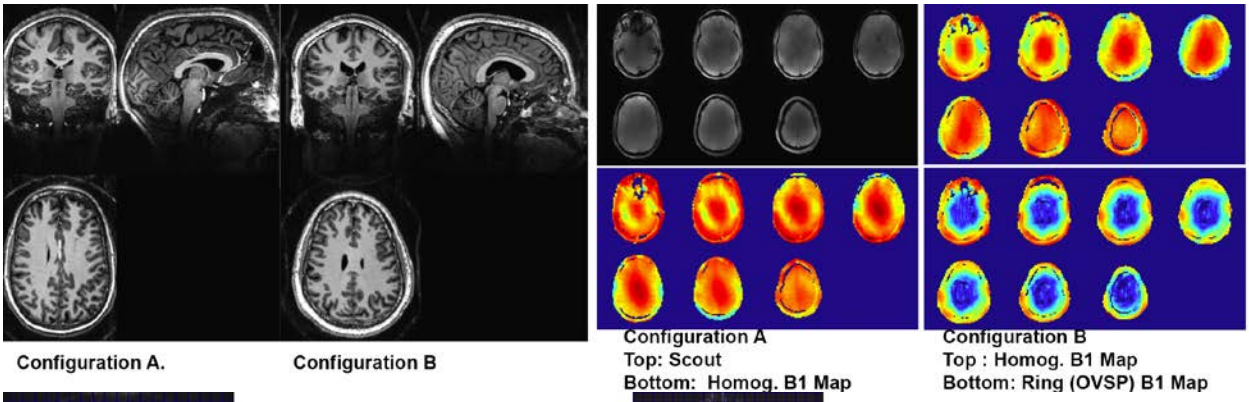

Conclusions: The 8x2 transceiver array provides for extended brain coverage, high homogeneity, and efficiency.

Functional MRI with multi-band multi-echo GE-EPI:

Enhanced BOLD contrast at high-susceptibility regions of brain

Tae Kim[1,2]*, Tiejun Zhao[3], and Kyongtae T. Bae[1,2]

Department of [1]Radiology and [2]Bioengineering, University of Pittsburgh, Pittsburgh, PA 15213

[3] Siemens MediCare USA, Siemens Medical Solution USA, INC., Pittsburgh, PA 15213

Functional MRI study is commonly performed by GE-EPI because of its high sensitivity to BOLD signal changes. However, GE-EPI method suffers from susceptibility-induced signal loss. This dephasing effect causes limited information in fMRI studies on regions of the cortex near field inhomogeneities such as amygdala, orbitofrontal cortex, and medial and inferior temporal lobes, which are associated with the processing of memory, decision-making, and emotional reactions. Voxel-wise weighted echo summation (WES) obtained from multi-echo acquisition improves susceptibility-induced signal loss in high susceptible area by weighting predominately from the shorter echo signal [1]. The use of thin slice can improve the local apparent T2* by reducing intravoxel spin dephasing effect. Thus, combination of thin slice summation with WES can improve both recovery of signal dropout and BOLD sensitivity. One potential drawback of aforementioned methods is long imaging acquisition time, and consequently the number of slices is limited within a reasonable TR, i.e. temporal resolution for fMRI studies. Recently, a multi-band (MB) excitation imaging technique was developed to increase the speed of data acquisition [2-4]. We applied this MB technique to accelerate imaging acquisition time. We compared tSNR and BOLD maps of conventional GE-EPI, multiband WES and multiband WES with thin slice summation for the whole brain.

Ten healthy volunteers (age: 34 ± 8, 6 males and 4 females) were studied using a 3T TIM Trio scanner (Siemens AG, Erlangen, Germany) with a built-in whole-body coil for the RF transmission and a 32-channel head coil (Siemens AG) for the RF reception. 20-s of breath-holding was performed twice for each run, using a block-design paradigm (60s-(20s)-40s-(20s)-50s; parentheses indicate breath-holding periods). Subjects were asked to hold their breath after exhaling to prevent a biphasic change. Anatomical image was acquired using a T_1-weighted magnetization prepared rapid gradient echo (MPRAGE) with TR = 1.5 s, TE = 3.19 ms, TI = 800 ms, FA = 8° and voxel size = 1 x 1 x 1mm^3. This fMRI study was acquired with three different conditions with randomized order. Experiment #1: conventional EPI, single band single echo (SBSE) was acquired with TR = 2.5 s, TE = 35 ms, flip angle (FA) = 68°, field of view (FOV) = 23 x 23 cm^2, matrix size = 64 x 64, slice thickness = 4 mm, and the number of slices = 30. Experiment #2: multiband multiecho (MBME) EPI technique used with the same parameters of experiment #1 except MB acceleration factor = 5 and TE = 17, 44.6, and 72.2 ms. Experiment #3: the same parameters were used as experiment #2 except slice thickness = 1 mm (MBMEthin) and the number of slices = 120 was acquired for the same brain coverage with experiment #1 and #2. For experiment #3, four consecutive slices were summated to match with 4 mm of slice thickness. For experiments #2 and #3, three-echo data was used to calculate T_2* value for each voxel, fitting with log-linear regression, and then a multi-echo dataset were combined for optimal functional contrast (~TE = T_2^*). For each voxel, WES maps were calculated using a factor, $w(T_2^*)_n = (TE_n \cdot \exp(-TE_n/T_2^*))/(\Sigma TE_n \cdot \exp(-TE_n/T_2^*))$ [1]. Temporal-signal-to-noise (tSNR) maps were calculated by dividing the mean of the corresponding time series by its standard deviation.

The susceptibility-induced signal dropout was markedly reduced with the summation of four neighboring thin-slices from the MBMEthin technique as compared with the thick-slice measurements from the MBME technique. The apparent R_2* (=1/T_2*) at all twelve regions was lower with the MBMEthin technique than that with the MBME. The differences between the MBME and MBMEthin techniques were more pronounced at

high susceptibility regions. As compared with conventional SBSE EPI, MBME increased the tSNR values at high susceptibility regions, such as the amygdala, orbitofrontal cortex, middle and inferior temporal lobes, while MBMEthin further enhanced the tSNR values at these regions. However, the tSNR values at other non-dropout regions of brain, including the frontal (excluding orbitofrontal) and occipital lobes, were comparable among the three methods, indicating the robustness of our implemented MB imaging method. The BOLD response maps to breath-hold stimulations were improved with the MBME method at the high-susceptibility regions including the amygdala, fusiform, hippocampus, orbitofrontal, inferior temporal, middle temporal, and temporal pole. Further enhancement with the MBMEthin method was apparent in the frontal pole and temporal pole regions.

References:

1. Posse et al., MRM 1999, 42, 82-97.
2. Moeller et al., MRM 2010;63(5):1144-1153.
3. Setsompop et al., MRM 2012;67(5):1210-1224.
4. Feinberg et al., PLoS One 2010;5(12):e15710

Gradient-echo EPI using a shim insert coil at 7T: Implication for BOLD fMRI.

Tae Kim, Yoojin Lee, Ajay Kurani, Hoby Hetherington, Jullie Pan, **University of Pittsburgh, Dept. of Radiology**

Purpose: B_0 inhomogeneity from differences in magnetic susceptibility is well known to result in signal reductions and spatial distortions in gradient echo BOLD echo planar imaging (GE-EPI) which increases linearly with field strength. However, the extent to which improved B_0 shimming can reduce these effects has not been quantitatively evaluated. In this report we evaluate the extent by which 1^{st} – 4^{th} degree/order shimming improves GE EPI BOLD imaging at 7T.

Methods: 8 healthy volunteers were studied at 7T (Siemens Magnetom) using an 8x2 (8coils/row x2 rows) transceiver array. The 16 coils were driven by 8 RF channels (amplitude, phase determined by RF shimming). The array was divided into 8 pairs of coils with each pair driven by a single independent RF channel using a 45° splitter. A 38cm ID shim insert coil consisting of 3^{rd}, 4^{th} degree and two 5^{th} degree shims with 10A shim supplies (Resonance Research Inc.) was used for higher degree shimming. B_0 mapping was performed using a 5 time point (1.0 to 8ms evolution times) multi-slice measurement with shim values calculated using a non-iterative least squares algorithm[1] (Bolero, *Bo l*oop *e*ncoded *r*eado*u*t). Single-shot GE-EPI was acquired with FOV 19.2×19.2 cm^2, matrix size 96×96, 2mm isotropic voxels, TR/TE 3.5 s/24 ms, FA 60° and 48 slices. To induce a BOLD signal response for the whole brain, a 21-sec breath-hold protocol was performed five times using a block-design paradigm (140s−[(21s)−35s]x5; parentheses indicates breath-hold period). Each run was repeated twice for 1^{st}&2^{nd} and 1^{st}-4^{th} degree/order shimming. R_2* was measured with multi-TE acquisition (TE 15, 20, 25, 30, 35 and 42ms). The B_0 induced pixel shifts were calculated by FSL FUGUE; all data processed with AFNI and FSL. MP2RAGE[2] images were used for anatomical registration using a voxel size 0.75mm^3 isotropic TR/TE 6s/3.1ms, TI =0.8s, and GRAPPA = 3.

Results and Conclusion: Fig. 1 shows GE-EPI with 1^{st}-2^{nd} and 1^{st}-4^{th} degree shimming (before B_0 distortion correction), demonstrating the decreased signal distortion with 1^{st}-4^{th}. Fig. 2A,B displays the calculated pixel shift maps from 1^{st}-2^{nd} and the 1^{st}-4^{th} shimmed data (n=8 subjects). From 8 subjects, the standard deviation of B_0 over the entire brain with higher order shimming decreased 26% (29.9 ± 4.5 Hz to 22.1 ± 3.8 Hz) for 1^{st}&2^{nd} vs. 1^{st}–4^{th} degree shimming). To visualize the regional improvement in B_0 homogeneity, pixels with $|B_0^{1\&2degree}| - |B_0^{1-4+degree}| \geq 10$Hz are overlaid on the anatomical image (Fig. 2C). Positive values (green to red) indicate regions where the field homogeneity improved with higher degree shims (e.g. high susceptibility regions such as anterior frontal and temporal lobes). Table 1 shows that with increasing improvement in B_0 homogeneity ($|B_0^{1\&2degree}| - |B_0^{1-4+degree}|$, in 10Hz ΔB0 bins), the number of activated pixels and strength of BOLD activation increases. Notably, this improvement is seen despite a modest improvement in R_2*. This is consistent with a mechanism whereby geometric distortion due to poor B_0 homogeneity (1^{st}&2^{nd} degree shimming) shifts white matter or CSF pixels onto gray matter or vice versa. This unwanted overlap alters BOLD signal. Improved homogeneity (1^{st}-4^{th} degree shimming) reduces this effect providing for more accurate activation. While at 2x2x2mm^3 resolution the R_2* was only modestly improved, our previous work using ~3x3x3mm^3 resolution showed substantial gains in signal intensity (related to R_2*) with high degree shimming. Thus although the mechanism for improvement depends on pixel size, high degree shimming provides for improvements for high and moderate resolution functional imaging at 7T.

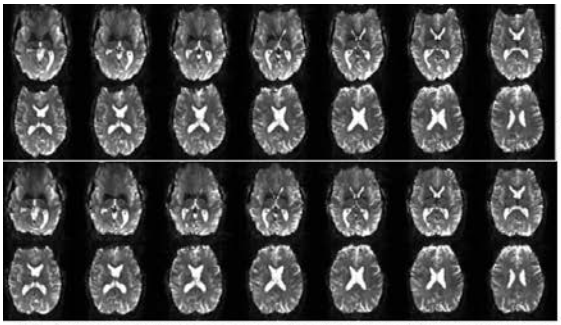

Fig. 1 GE EPI from same subject Top: 1st&2nd shimmed, Bottom: 1st-4th shimmed.

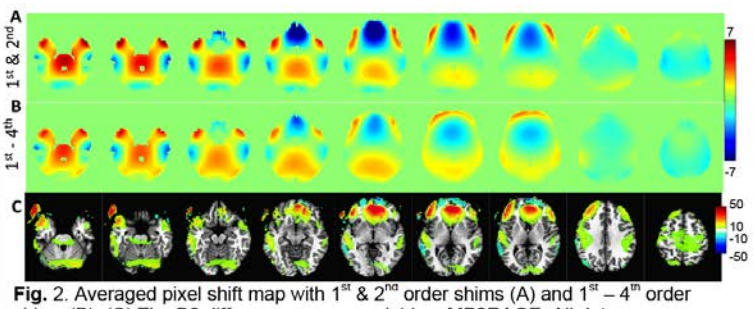

Fig. 2. Averaged pixel shift map with 1^{st} & 2^{nd} order shims (A) and 1^{st} – 4^{th} order shims (B). (C) The B0 difference maps overlaid on MP2RAGE. All data were averaged after normalization to Talairach space.

Table 1. Measured parameters with improvement of B_0 homogeneity (n = 8), $^{*}p< 0.05$, $^{**}p < 0.01$

ΔB0 bin	No. pixels in ROI	Pixel shift		R_2^*		% incr. Act. Pix	% incr. BOLD
		1^{st} & 2^{nd}	1^{st} - 4^{th}	1^{st} & 2^{nd}	1^{st} - 4^{th}	1^{st} - 4^{th}	1^{st} - 4^{th}
11-20	17738 ± 1682	1.1 ± 0.1	1.1 ± 0.1	40.0 ± 1.4	39.3 ± 1.6*	39.3 ± 61.9	6.7 ± 21.1
21-30	11079 ± 1635	1.4 ± 0.2	1.2 ± 0.1**	41.7 ± 1.4	40.7 ± 1.3**	38.7 ± 58.9	8.1 ± 20.3
31-40	5632 ± 795	2.1 ± 0.3	1.2 ± 0.1**	43.6 ± 1.6	42.3 ± 1.8**	39.4 ± 59.2	7.4 ± 20.1
41-50	2635 ± 367	2.5 ± 0.4	1.3 ± 0.2**	48.5 ± 2.5	46.6 ± 1.9*	32.8 ± 43.4	3.3 ± 25.1
51-60	1357 ± 330	2.8 ± 0.5	1.3 ± 0.3**	53.0 ± 4.5	50.5 ± 2.7	33.2 ± 38.9*	24.7 ± 23.1*
61-70	762 ± 242	2.9 ± 0.3	1.3 ± 0.2**	57.8 ± 5.6	54.8 ± 2.6	24.9 ± 30.2	20.8 ± 22.7*
71-80	457 ± 150	3.4 ± 0.4	1.5 ± 0.3**	61.5 ± 6.1	58.3 ± 3.5	15.4 ± 28.5	27.8 ± 57.5

References: 1. Pan JW, MRM . 2012. 2. Marques JP et al., Neuroimage 2010. 3. Kim et al. ISMRM 2013

7T WHOLE BRAIN MRI PROVIDES INCREASED STATISTICAL POWER FOR MORPHOMETRIC ANALYSIS OF NEUROANATOMY

Pardoe, H. R.[1]; Shin, W.[2]; Lowe, M.[2]; Hetherington, H.[3]; Kuzniecky, R.[1]; Pan, J.[3]
1. Neurology, New York University School of Medicine, New York City, NY, United States.
2. Cleveland Clinic, Cleveland, OH, United States.
3. University of Pittsburgh, Pittsburgh, PA, United States.

Rationale: The aim of this study is to quantify the benefit of 7T imaging for assessing neuroanatomical changes. Recent developments in 7T MRI allow for the acquisition of isotropic whole brain MRI with superior contrast and spatial resolution to 3T MRI. We used 7T MRI to measure hippocampal volume and vertex-wise cortical thickness, and compared these assessments with conventional 3T imaging. Power analyses were used to quantify the benefit of high field MRI by estimating the minimum volume or thickness difference that could be identified using 7T and 3T imaging.

Methods: Whole brain T1-weighted MRI was acquired at 7T and 3T (Siemens 7T whole body in pTx configuration; Siemens 3T Trio) in 9 subjects. The 7T data were acquired with a 8x2 16 channel transceiver, B1 shimmed for homogeneous mode imaging (Resonance Research Inc.). 3T data were acquired with a 32 channel head coil. The 3D 7T data used MP2RAGE with 4° and 5° flip angles, TR/TE 6s/3.16ms, GRAPPA 3, acquisition duration 9.5min, 750um isotropic. The 3T data used MPRAGE with 8° flip angle, TR/TE 1.56/3.2, GRAPPA 2, acquisition duration 5.1min, 1 mm isotropic. Freesurfer v 5.3 was used for subcortical segmentation and cortical surface modeling. The standard freesurfer processing stream was used for the 3T MRI. A previously published image processing protocol [1] was used for the 7T imaging data that allowed morphometric estimates to be assessed at the native resolution (0.75 mm isotropic). 7T and 3T across-subject variance estimates were used to calculate the minimum detectable effect size for hippocampal volume and vertex-wise cortical thickness using power analysis methods implemented in the R software package.

Results: An example of 7T and 3T images of the same subject are shown in Fig. 1. Across-subject variance was lower for hippocampal volumes and average cortical thickness when assessed at 7T compared with 3T imaging. Power analyses demonstrate that 7T imaging may be used to detect smaller hippocampal volume or cortical thickness changes than 3T imaging in group studies with equivalent numbers of participants (Figure 2 left). Conversely, the same effect size could be detected at 7T using lower numbers of participants than 3T. For example a hippocampal volume difference of 400 mm3 could be detected using 30 subjects at 3T or less than 10 subjects at 7T. Although there is an overall improvement in sensitivity for cortical thickness measurement at 7T across the cortex, some cortical regions have higher variance at 7T such as the lateral temporal cortical regions (Figure 2 right).

Conclusions: We have demonstrated that the higher resolution and contrast 7T imaging may be used to obtain quantitative morphometric estimates with lower variance than 3T imaging. Increased statistical power associated with 7T imaging will allow for the detection of subtle hippocampal sclerosis or focal cortical dysplasia, or the ability to identify neuroanatomical changes in smaller groups which will be beneficial for studying rare epilepsy syndromes.

[1] Lusebrink et al, Neuroimage (2013) 70:122-31
(no table selected)

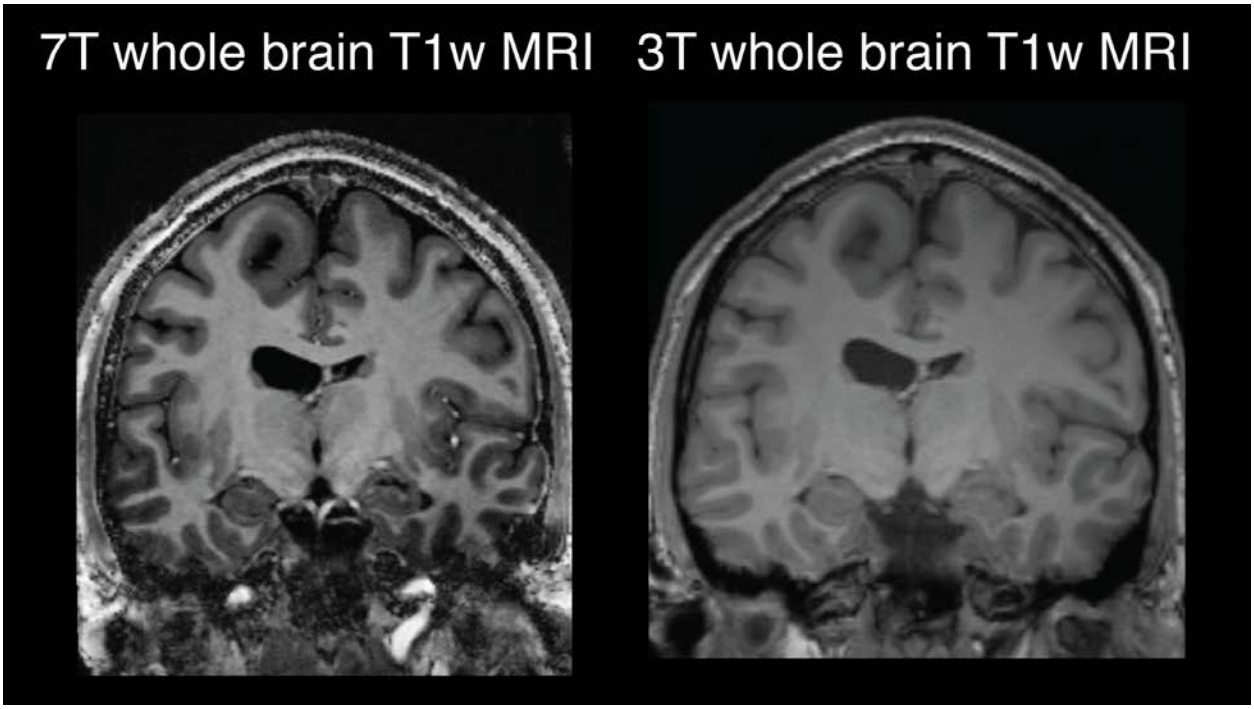

7T and 3T MRI in an epilepsy patient with right schizencephaly

Rosette spectroscopic imaging of human brain at 7T

C Schirda, T Zhao, JW Pan and HP Hetherington, MRRC University of Pittsburgh, Pittsburgh PA 15213

Introduction: For spectroscopic imaging, rosette sampling trajectories are advantageous compared with other rapid sampling strategies for their lower slew rate requirements (and thus decreased eddy current effects), full sampling over the signal decay window and greater spectral bandwidth for equal gradient constraints. The greater spectral bandwidth is especially useful for 7T. In this report we describe the integration of recent developments in transceiver array technology, high degree B_0 shimming with a rosette trajectory to achieve single slice spectroscopic imaging in ~2.5minutes.

Methods: A 7T Siemens Magnetom PTX Step 2 system and an 8x2 transceiver array (2 rows, 8coils/row) was used. For transmission, the 16 coils were driven by 8 independent RF channels (amplitude, phase determined by RF shimming). The two rows are paired superiorly-inferiorly, with each two-coil pair driven by a single independent RF channel using an equal amplitude 30^0 splitter. RF shimming was used to optimize two B_{1+} distributions; a ring distribution for outer volume suppression targeting the skull/skin for lipid suppression and a homogeneous distribution for excitation. A 38cm ID shim insert coil (Resonance Research Inc.) was used for higher degree shimming with a non-iterative least squares B_0 mapping algorithm (Bolero, *B0 l*oop *e*ncoded *r*ead*o*ut). The rosette acquisitions were collected with FOV=240mm^2 x10mm thick, matrix 24x24 for a nominal voxel size of 1cc, Gmax 5.2mT/m, Smax 45T/m/s, 40 shots with two temporal interleaves and a total acquisition time 2:12min. A water reference image was acquired with the same parameters with TR = 0.37s. The rosette acquisition was run at nominal 1cc voxel resolution to allow comparison to standard single slice spectroscopic imaging acquired with 14.5min with the same parameters. For both acquisitions, a TR/TE 1.5s/40ms spin echo was performed with pre-spin echo suppression of lipids (B_{1+} ring distribution) and water (B_{1+} *homogeneous distribution). The* reconstruction used a Kaiser-Bessel kernel with a two-fold oversampled grid for the gridding and 2D hamming spatial filtering. Channel recombination was performed using the phases from the water reference data. The time domain data was then analyzed by LCM covering 0.2 to 4.0ppm and a spectroscopic image of NAA was generated.

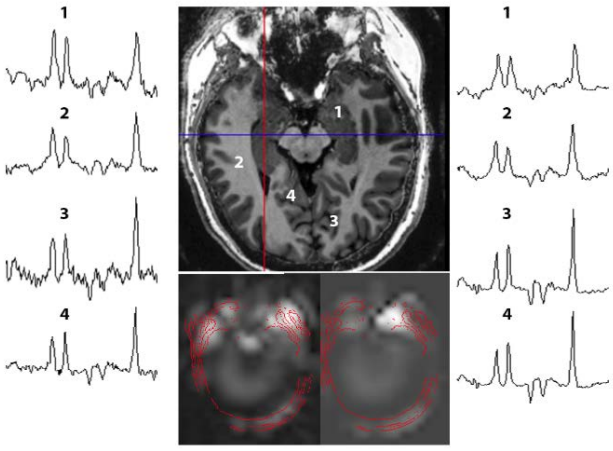

Fig 1: Co---registered slice from a 3D MP2RAGE acquisition, displaying spectra from 4 locations. The spectra from those locations are displayed to the left (rosette) and right (conventional phase encoding) acquisitions. Integrated images of NAA are displayed below the anatomical image for the rosette (left) and conventional acquisition (right). The bright region anterior to the mid-brain and about the orbits is from residual lipid signals associated with blood flow and large fat deposits.

Results and Conclusion: Figure 1 shows data from a temporal lobe study comparing the 14.5 min conventional 2D encoded acquisition (right) with the 2.25 min. rosette acquisition (left). The SNR of the conventional phase encoding study is ~2 to 3 times that of the rosette study, consistent with the 6-7 fold longer acquisition time. The reduced gradient strengths utilized by the rosette acquisition minimize eddy current effects, generating spectra of similar spectral resolution to that of the conventional acquisition. The high SNR at 7T, sensitivity of the transceiver array and 1st-4th degree shimming provides readily interpretable data for major singlets throughout the slice in 2.5 min. of acquisition. This includes the most anterior regions of the hippocampus (1), lateral temporal lobe (2) and occipital lobe (3,4). Rosette spectroscopic imaging provides a fast accurate method for MRSI at 7T in patient populations where subject compliance may be challenging.

Association of Breast DCE-MRI Contrast Enhancement Kinetics Quantified from Normal Breast Tissue with Breast Cancer Risk

[1]Shandong Wu, PhD, [1,2]Wendie A. Berg, MD, PhD, [1,2]Margarita L. Zuley, MD, [3]Brenda F. Kurland, PhD, [2,4]Rachel C. Jankowitz, MD, [1]David Gur, ScD, [1,2]Jules H. Sumkin, DO.
[1]Department of Radiology, University of Pittsburgh
[2]Magee-Womens Hospital of University of Pittsburgh Medical Center
[3]University of Pittsburgh Cancer Institute, Department of Biostatistics, University of Pittsburgh
[4]Department of Medicine, University of Pittsburgh

OBJECTIVES: To investigate association of contrast enhancement kinetic variables quantified from normal breast tissue in breast dynamic contrast-enhanced magnetic resonance imaging (DCE-MRI) with breast cancer in a case-control study.

MATERIALS AND METHODS: Under a Health Insurance Portability and Accountability Act compliant and Institutional Review Board-approved protocol, DCE-MRIs were retrospectively analyzed for 51 cancer cases and 51 controls with biopsy-proven benign lesions, matched by age and year- of-MRI. Applying fully-automated computer algorithms on pre-contrast and multiple post-contrast MR sequences, two contrast enhancement kinetic variables, namely wash-in-slope and signal-enhancement-ratio, were quantified from normal breast tissue of the contralateral breasts of both cancer cases and controls. Conditional logistic regression was employed to assess association of these two measures with breast cancer, with adjustment for other risk factors including mammographic breast density and MRI background parenchymal enhancement (BPE). Area under the receiver operating characteristic curve (AUC) was used to assess classification ability of the two measures in distinguishing cancers from controls.

RESULTS: When both kinetic measures were included in conditional logistic regression analysis, odds ratio of breast cancer was 1.7 (95% CI: 1.1, 2.8; p=0.017) for wash-in-slope-variance and 3.5 (95% CI: 1.2, 9.9; p=0.019) for signal-enhancement-ratio-volume, respectively. These odds ratios were similar to their respective univariate analysis, and remained significant after adjustment for menopausal status, family history, mammographic density, and BPE. In the classification of cancers from controls, the combination of the two measures achieved an unadjusted AUC of 0.71, significantly (both p=0.005) outperformed either of them alone (AUC=0.65 for wash-in-slope-variance and 0.63 for signal-enhancement-ratio volume).

CONCLUSIONS: Quantitative measures of wash-in-slope and signal-enhancement-ratio are jointly associated with breast cancer risk, even after adjustment for mammographic density and MRI BPE.

Connectometry: a statistical approach harnessing the analytical potential of the local connectome

Fang-Cheng Yeh[1,*], David Badre[2], and Timothy Verstynen[1,*]

[1]Department of Psychology, Carnegie Mellon University, Pennsylvania, USA;

[2]Department of Cognitive, Linguistic and Psychological Sciences, Brown University, Rhode Island, USA;

ABSTRACT

Here we introduce the concept of the *local* connectome: the degree of connectivity between adjacent voxels within a white matter fascicle defined by the density of the diffusing spins. While most human structural connectomic analyses can be summarized as finding global connectivity patterns at either end of anatomical pathways, the analysis of local connectomes, termed connectometry, tracks the local connectivity patterns along the fiber pathways themselves in order to identify the subcomponents of the pathways that express significant associations with a study variable. This bottom-up analytical approach is made possible by reconstructing diffusion MRI data into a common stereotaxic space that allows for associating local connectomes across subjects. The substantial associations can then be tracked along the white matter pathways, and statistical inference is obtained using permutation tests on the length of coherent associations and corrected for multiple comparisons. Using two separate samples, with different acquisition parameters, we show how connectometry can capture variability within core white matter pathways in a statistically efficient manner and extract meaningful variability from white matter pathways, complements graph-theoretic connectomic measures, and is more sensitive than region-of-interest approaches.

Childhood Adversity Predicts the Structural Integrity of Limbic White Matter in Combat Veterans

Layla Banihashemi[1], Lei K. Sheu[2], Peter J. Gianaros[2], Anne Germain[1], Ryan J. Herringa[1,3]

[1]Department of Psychiatry, University of Pittsburgh, Pittsburgh, Pennsylvania 15213, USA

[2]Department of Psychology, University of Pittsburgh, Pittsburgh, Pennsylvania 15260, USA

[3]Department of Psychiatry, University of Wisconsin School of Medicine and Public Health, Madison, WI 53719, USA

Childhood adversity confers risk for mood and anxiety disorders, including post-traumatic stress disorder (PTSD). In military veterans, evidence suggests that childhood and later-life trauma may interact to yield enhanced vulnerability to PTSD. However, limbic brain changes associated with childhood adversity are particularly unclear in veteran populations. Here, we examined childhood adversity-related differences in the structural integrity of limbic white matter pathways among veterans with post-traumatic stress symptoms. Participants were male Operations Enduring and Iraqi Freedom combat veterans (n=28). Structural integrity measures were extracted *a priori* from five limbic regions of interest using diffusion tensor imaging. Hierarchical linear regressions tested whether different forms of childhood trauma were associated with structural integrity measures adjusting for age, race, depressive symptoms, PTSD symptoms and traumatic brain injury. Our findings showed: 1) childhood physical abuse was associated with structural integrity measures within every limbic tract examined, and 2) all subtypes of childhood trauma examined were associated with decreased fractional anisotropy. Such childhood adversity-related differences in limbic pathways may contribute to increased vulnerability to developing psychopathology later in life.

Altered resting state connectivity in behaviorally and emotionally dysregulated youth in the Longitudinal Assessment of Manic Symptoms (LAMS) study

Genna Bebko[a], Michele Bertocci[a], Henry Chase[a], Amanda Dwojak[a], Lisa Bonar[a], Jorge Almeida[a], Susan Beth Perlman[a], Amelia Versace[a], Claudiu Schirda[a], Michael Travis[a], Mary Kay Gill[a], Christine Demeter[b], Vaibhav Diwadka[c], Jeffrey Sunshine[b], Scott Holland[d], Robert Kowatch[e], Boris Birmaher[a], David Axelson[e], Sarah Horwitz[f], Thomas Frazier[g], Lawrence Eugene Arnold[e], Mary Fristad[e], Eric Youngstrom[h], Robert Findling[b,i], and Mary Louise Phillips[a]

[a]Department of Psychiatry, Western Psychiatric Institute and Clinic, University of Pittsburgh Medical Center, Pittsburgh, Pennsylvania, United States of America
[b]University Hospitals Case Medical Center/Case Western Reserve University, Cleveland, Ohio, United States of America
[c]Department of Psychiatry and Behavioral Neuroscience, Wayne State University, Detroit, Michigan, United States of America
[d]Cincinnati Children's Hospital Medical Center, University of Cincinnati, Cincinnati, Ohio, United States of America
[e]Department of Psychiatry, Ohio State University, Columbus, Ohio, United States of America
[f]Department of Child and Adolescent Psychiatry, New York University School of Medicine, New York, New York, United States of America
[g]Pediatric Institute, Cleveland Clinic, Cleveland, Ohio, United States of America
[h]Department of Psychology, University of North Carolina at Chapel Hill, Chapel Hill, North Carolina, United States of America
[i]Department of Psychiatry, Johns Hopkins University, Baltimore, Maryland, United States of America

Background: The Research Domain Criteria (RDoC) advocates using a dimensional research approach to study transdiagnostic pathophysiological processes in psychiatric disorders. Studying brain-behavior relationships using neuroimaging techniques, such as resting state functional connectivity (RSC), is ideally suited to follow the RDoC framework.

Significance: Our findings add to the growing body of literature in support of the RDoC dimensional research approach to the transdiagnostic study of psychiatric disorders.

Methods: Following the RDoC dimensional research approach, we examined relationships between RSC and symptom dimensions (dimensional severity measures of behavioral and emotional dysregulation [PGBI-10M], mania [K-MRS], depression [K-DRS], anxiety [SCARED]) and diagnostic categories (Bipolar Spectrum Disorders, Attention Deficit Hyperactivity Disorder, Anxiety Disorders, Disruptive Behavior Disorders) in behaviorally and emotionally dysregulated youth in the Longitudinal Assessment of Manic Symptoms (LAMS) study (n=42). RSC analyses examined functional coupling between an amygdala seed region and a priori regions of interest: prefrontal cortex (BA10, BA11, BA24/32, BA47), striatum (caudate head and body, putamen, and ventral striatum), and insula.

Results: Regardless of diagnosis and after accounting for demographic variables, RSC showed significant negative relationships with two symptom dimensions across all LAMS youth ($p<.05$ voxelwise, $p<.05$ corrected): 1) PGBI-10M and the amygdala-left posterior insula/bilateral putamen RSC; and 2) K-DRS and amygdala-right posterior insula RSC. There were no significant relationships between diagnostic categories and resting state connectivity.

Conclusions: Decreased amygdala-posterior insula RSC was significantly associated with increased severity of symptom dimensions across all LAMS youth, regardless of diagnosis, suggesting intrinsic functional uncoupling of key neural circuitry involved in emotion processing and regulation.

The insula's functional connectivity to the default mode network is uniquely altered by pain perception

Christopher Becker, MA, Keigh Vogt, MD, PhD, James Ibinson, MD, PhD

Background: Multiple studies across imaging modalities suggest the insula has a key role in pain processing. Recent work using functional connectivity MRI (fcMRI) during painful and innocuous thermal stimulation demonstrated anatomically different connectivity: the anterior insula (aIns) was more strongly correlated to the anterior cingulate cortex (ACC), while the posterior insula (pIns) better correlated to the primary somatosensory (S1) and motor (M1) cortices. Similarly, our prior work showed altered connectivity of the pIns to default mode network (DMN), and the posterior cingulate cortex (PCC) in particular, during painful acute electric nerve stimulation versus rest.

Methods: In this work, we tested a longer (30 min) tonic capsaicin application to determine if the same insula-to-DMN fcMRI alterations would be found. 3 T BOLD data was acquired in 6 healthy adults during rest and at the end of a 30 minute capsaicin solution application to the left volar forearm. Functional connectivity was determined using the CONN toolbox for SPM. aIns and pIns seed regions were defined on the standard MNI-152 brain and transformed back for each individual subject.

Results: Group average functional connectivity maps demonstrated strong rest vs pain differences in connectivity between both seeds of the insula and the PCC, with the pIns differences being more significant.

Conclusions: Our data suggests that the insula shows dynamic changes in connectivity during tonic pain, which may provide a means of differentiating between rest and pain states.

An examination of change in neural function supporting change in measures of dysregulation

Michele A. Bertocci PhD[1], Genna Bebko PhD[1], Amanda Dwojak BS[1], Cecile D Ladouceur PhD[1], Jay C. Fournier PhD[1], Satish Iyengar PhD[2], Amelia Versace MD[1], Susan B. Perlman PhD[1], Jorge R. C. Almeida MD PhD[12], Michael J Travis MD[1], Mary Kay Gill MSN[1], Lisa Bonar BS[1], Claudiu Schirda PhD[1], Vaibhav A. Diwadkar PhD[4], Jeffrey L. Sunshine MD PhD[3], Scott K. Holland PhD[5], Robert A. Kowatch MD PhD[6], Boris Birmaher MD[1], David Axelson MD[6], Sarah M. Horwitz PhD[7], Thomas Frazier PhD[8,] L. Eugene Arnold MD MEd[9], Mary A. Fristad PhD[8], Eric A. Youngstrom PhD[10], Robert L. Findling MD, MBA[3,11], and Mary L. Phillips MD, MD (Cantab)[1]

[1]Department of Psychiatry, Western Psychiatric Institute and Clinic, University of Pittsburgh Medical Center, University of Pittsburgh
[2]Department of Psychology, University of Pittsburgh
[3]University Hospitals Case Medical Center/Case Western Reserve University
[4]Department of Psychiatry and Behavioral Neuroscience, Wayne State University
[5]Cincinnati Children's Hospital Medical Center, University of Cincinnati
[6]The Research Institute at Nationwide Children's Hospital
[7]Department of Child Psychiatry, New York University School of Medicine
[8]Department of Psychiatry, Ohio State University
[9]Department of Psychiatry and Behavioral Health, Ohio State University
[10]Department of Psychology, University of North Carolina at Chapel Hill
[11]Department of Psychiatry, Johns Hopkins University
[12]Alpert Medical School, Brown University

Background: Identification of neural markers that change over time with changes in behavioral and emotional dysregulation may aid in understanding psychopathology. We examined the relationships between changes in emotion regulation neural function and changes in clinical, parental, and self-report measures of dysregulation.

Methods: Forty-two behaviorally and emotionally dysregulated youth completed two functional neuroimaging assessments (M=21.3 months apart). At each scan, youth performed an emotional regulation task, psychiatric assessments, and parental and self-report measures of psychopathology. We used multiple response Gaussian regression penalized with an elasticnet to identify an emotion regulation neural model that changes in conjunction with changes in measures of depression, mania, anxiety, affect lability, and positive mood and energy simultaneously, after accounting for clinical, medication, and demographic variables.

Results: Analyses revealed non-zero coefficients over time between change in our outcome measures and change in activity in two neural regions: right amygdala and left ventrolateral prefrontal cortex (vlPFC). There were consistent patterns of increased amygdala and vlPFC activity associated with worsening of depression, and affect lability. There were interactions between right amygdala and left vlPFC activity related to mania, anxiety, and positive mood and energy scales. Specifically, increased right amygdala and decreased left vlPFC activity was associated with worsening mania symptoms while the opposite pattern was shown for worsening anxiety and positive mood and energy psychopathology in behaviorally and emotionally dysregulated youth, after accounting for baseline clinical measures.

Conclusions: These data identify potential target areas for understanding neural changes associated with dysregulated emotions and behaviors.

R01 MH073953

Long-term skill learning is associated with a reorganization of cortical motor representations in humans

Patrick Beukema[1,3], & Timothy Verstynen[2,3]

[1]Center for Neuroscience

University of Pittsburgh

Pittsburgh, PA 15260

[2]Department of Psychology

[3]Center for the Neural Basis of Cognition

Carnegie Mellon University

Pittsburgh, PA 15213

Background/Significance: Skilled performance of movement is associated with increases in motor efficiency. One of the hallmarks of increased efficiency is thought to be a reorganization of multiple individual motor units to a single executable chunk (Lashley, 1951). However, the neural substrate of this reorganization is unknown. Here we examined where the representations of individual finger movements evolve with learning.

Methods: Subjects underwent two fMRI scans to localize individual digit representations before and after training (5 weeks) on a complex sequential motor task. The sequence of actions was designed to illicit higher frequency pairings between specific digits. Representational dissimilarity analysis was used to identify the cortical regions where distances between individual fingers changed following training.

Results: We observed a reorganization of the representations of the finger movements following long-term training, decreasing in primary motor cortex and increasing in somatosensory and rostral parietal regions.

Conclusions: Long-term skill acquisition reorganizes motor representations and may partly underlie the observed behavioral characteristics of efficient movement production.

References:

Lashley, K. (1951). The problem of serial order in behavior. *1951*, (7), 112–147. doi:10.1093/rfs/hhq153

Combining MRI and Ultrasound: the Brain Tissue Pulsatility Imaging to assess the biomechanical properties of the brain.

Thomas Desmidt[1,2,3]

[1]Geriatric Psychiatry Neuroimaging Lab, Pittsburgh, USA

[2]UMRS INSERM U930, Tours, France

[3]CHRU de Tours, Tours, France

The recent development of ultrasound (US) imaging technology, both in probe technology and signal processing, has made possible the development of the so-called Tissue Pulsatility Imaging (TPI). The main principle of TPI is to record an US sequence of the natural movements, including movements of the brain (Brain Tissue Pulsatility – BTP), using a modern echographic device in echo-B mode with a probe positioned on the temporal window of the skull with support of a neuronavigation system. It allows for a very high spatio-temporal resolution assessment (micrometers/milliseconds) of the brain biomechanical properties related to cerebral blood flow.

TPI has been validated on healthy volunteers and more recently on depressive patients, younger patients showing an increased BTP whereas older patients showing a decreased BTP. Unpublished yet results also indicate that Alzheimer's disease patients show an increased BTP and patients with orthostatic hypotension a decreased BTP. Moreover, we have been able to combine TPI with MRI thanks to the neuronavigation system (video of the technology available at: http://cic-it-tours.fr/recherche-clinique-translationnelle). This allows for a multimodal assessment of the brain physiology, US assessing for accurate displacements and MRI for anatomical localization. With this technological coupling, we found that BTP was inversely correlated with white matter hyperintensities load and was decreasing with age.

Eventually, the combination of the US TPI with MRI may allow to overcome some of the MRI limitations, including higher spatio-temporal resolution, lower cost, non-invasive procedure and may allow for an easier use in clinical routine.

Age-related changes in the neural substrates underlying face processing in autism

Jennifer Fedor, BS; Dhruv Kohli; Andrew Lynn, BS; William Foran, MS; Beatriz Luna, PhD; Kirsten O'Hearn, PhD

Department of Psychiatry, University of Pittsburgh School of Medicine

Background: Face recognition improves from adolescence to adulthood in typically developing (TD) individuals, but not in those with autism (ASD). We hypothesized that this differential development would also be evident in the fusiform face area (FFA), a region underlying face processing. The current study examined age-related changes in FFA activation during face memorization and recognition in TD and ASD.

Significance: This study provides insight into how the brain changes during typical development, whether this is related to improved face recognition, and how these developmental mechanisms differ in ASD.

Methods: We analyzed 28 children, 32 adolescents, and 28 adults with and without ASD. Participants completed a modified Cambridge Face Memory Task (CFMT), during which six faces are memorized and subsequently recognized. FFA regions of interest (ROIs) were defined using NeuroSynth. We performed 2 (group) x 3 (age group) ANOVAs to examine group- and age-related differences in FFA activation separately during memorization and recognition.

Results: During memorization, activation in L FFA was greater in TD than in ASD, although there was no effect of age. Follow-up t-tests revealed that group differences were significant in childhood, with greater activation in TD than ASD, but not in adolescence or adulthood. Activation was similar across group and age in R FFA during memorization and bilateral FFA during recognition.

Conclusions: Our work suggests that FFA activation in ASD is generally similar to TD, and does not change across age. However, differences in L FFA activity during memorization may reflect atypical face processing in children with ASD.

Adolescents' neural response to social reward and emotional closeness during naturalistic social interactions

Author(s): Luis E. Flores, Jr.[1,2], Jennifer S. Silk[3], Marigrace Ambrosia[2], & Erika E. Forbes[2]
Affiliation(s): [1]VISN 4 Mental Illness Research, Education and Clinical Center (MIRECC), VA Pittsburgh Healthcare System; [2]Department of Psychiatry, University of Pittsburgh School of Medicine; [3]Department of Psychology, University of Pittsburgh

BACKGROUND: Emotional closeness (Flores & Berenbaum, 2014) and function in neural reward circuitry (Forbes & Dahl, 2012) play important roles in depression. These factors may not be independent, and individuals who experience less closeness may also demonstrate altered neural response to social rewards.

SIGNIFICANCE: Investigating this relation may elucidate their roles in adolescent depression, especially given that social acceptance is particularly valued in adolescence.

METHODS: A sample of 34 healthy adolescents were called 28 times over two-weeks and asked how close they felt with whom they were interacting. They also participated in a social reward fMRI task in which they received feedback about whether other adolescents – represented by standardized faces – think they would like them (Davey et al., 2010). Positive/reward trials, which were grouped into blocks, indicated that they liked the participant and neutral trials indicated that "they had not yet rated the participant." We used a Siemens 3T TIM Trio scanner and SPM8 for preprocessing and analyses.

RESULTS: Adolescents who experienced more closeness during social interactions exhibited greater neural response to social reward in certain brain regions (i.e., right temporoparietal junction, TPJ, and right ventrolateral prefrontal cortex, VLPFC) that play important roles in social processing.

CONCLUSIONS: Greater activation in TPJ and VLPFC suggest that adolescents who experience more emotional closeness may engage in more perspective taking and positive affect and behavior regulation in the context of social reward (e.g., positive peer feedback). Further, engagement in these prosocial processes during positive social interactions may facilitate the experience of emotional closeness.

Neural correlates of risky decision-making predict early recovery outcomes in substance dependent individuals.

Sarah E. Forster, PhD[1,2,3], Peter R. Finn, PhD[1], & Joshua W. Brown, PhD[1]

[1] Indiana University, Department of Psychological and Brain Sciences, [2] VA Pittsburgh Healthcare System, [3] University of Pittsburgh, Department of Psychiatry

Background: Substance use disorders are chronic, relapsing conditions and reliable predictors of treatment outcome have not yet been characterized. Recently, patterns of neural activity have been identified as potential neuroprognostic indicators in substance use disorders.

Significance: Candidate neuromarkers of relapse risk have primarily been explored in relatively homogenous research samples and have not been studied in naturalistic samples, typical of community-based treatment settings. The current study sought to identify brain-based predictors of treatment outcome in a mixed sample of substance dependent individuals, without exclusion of common psychiatric comorbidities. The predictive utility of brain-based measures was also assessed relative to clinical indicators, cognitive-behavioral performance, and self-report measures.

Methods: The study utilized a prospective clinical outcome design in the context of a longitudinal functional magnetic resonance imaging study using the Balloon Analog Risk Task (BART). Twenty-three substance dependent individuals were recruited upon treatment engagement, completed baseline assessments within 1-4 weeks of abstinence, and were followed for three months.

Results: Using voxel-level predictive modeling and leave-one-out cross-validation analysis, an increased response to negative feedback in bilateral amygdala and anterior hippocampus (Amyg/aHipp) at baseline was found to predict greater substance use over the 3 month study interval. This effect withstood inclusion of significant non-brain-based covariates. A larger response to negative feedback in bilateral Amyg/aHipp was also associated with faster reward-seeking responses after negative feedback.

Conclusions: The current findings suggest that brain-based assessments can effectively characterize relapse risk in a naturalistic sample of substance dependent individuals and may have clinical utility in community-based treatment settings.

The development of white matter microstructure and intrinsic functional connectivity between the amygdala and ventromedial prefrontal cortex

Maria Jalbrzikowski[1], Bart Larsen[2], William Foran[1], Finnegan Calabro[1], Beatriz Luna[1,2,3]

[1]University of Pittsburgh, Department of Psychiatry

[2]University of Pittsburgh, Department of Psychology

[3]University of Pittsburgh, Department of Pediatrics

Background. Functional and structural connectivity between the amygdala and ventromedial prefrontal (vmPFC) regions is compromised in multiple psychiatric disorders. Most psychiatric disorders develop during adolescence and multiple cognitive functions associated with amygdala-vmPFC connectivity continue to mature through adolescence; thus, it is essential to characterize how amygdala-vmPFC connectivity changes during typical development.

Significance. It is unknown whether precise sub-regions in the amygdala and vmPFC follow differential growth trajectories in structural and functional connectivity in late childhood, adolescence, and adulthood. Furthermore, it has not been determined whether development of white matter microstructure between the amygdala and vmPFC is related to development of amygdala-vmPFC functional connectivity.

Methods. We examined the development of amygdala-vmPFC intrinsic functional connectivity and white matter microstructure using resting state fMRI and diffusion-weighted imaging and from late childhood to early adulthood (10-30 years) on 255 individuals (1-3 time points). Non-linear regression models were used to examine the effects of age on amygdala-vmPFC connectivity. Time-varying effect models were used to assess changes in the associations between structural and functional amygdala-vmPFC connectivity.

Results. Functional connectivity between the amygdala and rostral anterior cingulate and subgenual cingulate significantly decreased from late childhood to early adulthood (between 10-23 years). White matter microstructure, as measured by generalized fractional anisotropy, significantly increased during this time (between 10-20 years).

Conclusion. Functional and structural connectivity between the amygdala and sub-regions of the vmPFC (e.g., rostral anterior cingulate and subgenual cingulate) show developmental changes from late childhood to early adulthood. These changes may be relevant to the appearance of clinical features associated with multiple psychiatric disorders.

The development of convergent corticostriatal structural connectivity during adolescence

Bart Larsen[1,2,3], Timothy Verstynen[3,5], Fang-Chen Yeh[6], Beatriz Luna[1,3,4]

1. Laboratory of Neurocognitive Development, 2. Psychology, 3. Center for the Neural Basis of Cognition, 4. Psychiatry, University of Pittsburgh; 5. Psychology, 6. Biomedical Engineering, Carnegie Mellon University

Adolescence is a stage of development characterized, in part, by heightened sensation seeking and continued development of cognitive ability. This unique behavioral profile is thought to be driven by relative rates of maturation of corticostriatal functional brain systems and their integration. The striatum contains primary input nuclei for cortical projections into the basal ganglia and serves as a hub of integration for distributed cortical systems. Here we investigate the development of convergent corticostriatal projections from cortical functional brain systems involved in limbic/reward-processing (cortical limbic system) and cognitive control (fronto-parietal and dorsal attention systems) using diffusion-weighted imaging and deterministic fiber-tracking in a large cross-sectional sample of adolescents and young adults (N = 231; range 10-31). The degree of convergence between the limbic and the dorsal attention and fronto-parietal networks differed as a function of age. In early adolescence, limbic input was proportionally greater than dorsal attention input to bilateral ventral putamen, and proportionally greater than fronto-parietal input in the right anterior putamen. As the dorsal attention and fronto-parietal networks are largely associated with top-down cognitive control function, this pattern of results suggests a greater weighting of limbic vs. control inputs during early adolescence that changes to predominance of control inputs in adulthood. This developmental pattern may contribute to increased sensation seeking behavior early in adolescence and developmental reduction of variability in cognitive control ability into early adulthood.

Developmental Increases in Phase Synchrony Between Human Functional Brain Networks

S. Marek[1,2,3], K. Hwang[4], A. Ghuman, B. Luna[1,2,3,5,6]

University of Pittsburgh Medical Center[1], Center for Neuroscience[2], Center for the Neural Basis of Cognition[3], Helen Wills Neuroscience Institute at University of California Berkeley[4], Department of Psychiatry[5], Department of Psychology[6]

Advances in resting state fMRI have revealed the human brain is organized into functional brain networks, which display a protracted development. However, a neurally based account of these maturational changes remains unclear. Here, we aimed to study the development of resting state functional brain networks using MEG to probe developmental changes network development using phase synchrony as our measure of connectivity. We hypothesized increased cortical synchrony in both alpha and beta frequency bands, mainly driven by between-network interactions, indicating increased network integration. We collected 5 minutes of resting state MEG data room 68 subjects, ranging in age from 14-31 years. Resting state data was first filtered into frequency bands, ranging from 1-40Hz. Next, for each subject we calculated a phase locking value (PLV) between every cortical ROI pair. Supporting our first hypothesis, there was a significant positive linear relationship between synchrony and age in the alpha band and high beta band across cortical networks. In both alpha and beta bands, this effect mainly was driven by between-network interactions. Significant between-network increases tended occur between frontal association areas and other brain networks, including the visual and default mode networks. Taken together, enhanced integration of synchronized phase relationships between functional brain networks may be a key factor facilitating maturation from adolescence to adulthood.

Reduction of neural variability within cognitive and motor systems supports developmental improvements in working memory performance

David Montez, Daniel Simmonds, and Beatrice Luna

Working memory (WM) improves through adolescence largely due to age related decreases in the variability of responses.The neural basis for improvements in the reliability of WM performance is not well understood. The present study aimed to characterize trial-to-trial behavioral variability that can be attributed to variability occurring within purely motor or purely cognitive processes and to characterize the relative changes in their contribution to behavioral variability at different ages. We examined a mixed longitudinal cohort of subjects, between the ages of 8 and 30, as they performed a variant of the memory-guided saccade task during fMRI acquisition.We identified a set of canonical BOLD signal brain states, or whole-brain patterns of activity, that are associated with eye-movement motor responses, working memory maintenance, and memory guided eye movements.We applied dimensionality reduction techniques to assess subject-level trial-to-trial variability of recruitment of networks supporting WM maintenance and retrieval as well as oculomotor performance.The results of our analyses demonstrate that performance of a spatial WM task relies on measurable independent contributions from motor and cognitive brain states. Variability in performance on individual trials is the result of differences in the degree to which motor and cognitive brain states are expressed on individual trials. We provide evidence that the magnitude of brain state variability in oculomotor systems is approximately fixed by late childhood but cognitive brain state variability —that variability associated with the maintenance and retrieval of spatial information— continues to decrease during the same time. We therefore conclude that the primary driver of reduced behavioral variability during adolescent development is the continued refinement of cognitive- and not occulomotor- related brain systems.

Investigation of functional baseline neuronal specificity and small-scale network during resting status in human primary motor cortex at 7T

Chan Hong Moon, Ph.D., [1,*] Jung-Hwan Kim, B.S., [1, 2] and Kyongtae Ty Bae, M.D., Ph.D. [1,2]

[1] Department of Radiology, University of Pittsburgh, 3362 Fifth Ave., Pittsburgh, PA 15213, USA; [2] Department of Bioengineering, University of Pittsburgh, 300 Technology Dr., Pittsburgh, PA 15213, USA

Background: Source of BOLD activation during resting-sate fMRI (rfMRI) is controversial at 7T, so the sensitivity to small neuronal activation such as brain baseline function is unclear. Small-scale connectivity research (e.g., within same functional domain) is relatively rare compared to large-scale connectivity study, possibly due to low BOLD sensitivity or/and low specificity. In this study, we investigated sources of rfMRI BOLD and possible detection of small-scaled connectivity in motor cortex by using high-field 7T.

Significance: It is critical to understand rfMRI BOLD sources, and study the specificity/sensitivity to small neuronal response at 7T. In addition, it is an urgent issue to investigate practical/potential advantages of 7T compared to 3T in neuroscience research.

Methods: All imaging was performed at 3T and 7T human scanner with multi-channel RF receiver. High- and low-resolution (1.6 vs. 3 mm) fMRI were done in primary motor area at both magnets during hand-grasp task and resting-state condition. Activation patterns were measured by using independent component analysis (ICA), and the results were compared for task vs. resting-state, 3T vs. 7T, and high vs. low-resolution, with regard to spatial distribution and functional connectivity.

Results: Activation patterns of task and resting-state fMRI were coincident each other. High-resolution rfMRI only at 7T could differentiate the activation source of BOLD in gray matter and draining veins, and showed the signals were dominant in surrounding vessels even at 7T. Hemispheric connection of baseline motor function was well detected in all rfMRI data, but separation of the connectivity between left and right hemisphere was consistently observed under high-signal BOLD at 7T.

Conclusions: rfMRI BOLD activation source at 7T are dominated by draining artifacts, but located always near the activated gray mater region. A large-scale connection between two hemispheres can be decomposed to smaller-scale functional connection by using 7T. Effect of draining artifact and BOLD strength on detectability of small-scale brain connectivity needs to be further studied.

3970

Diffusion reconstruction by combining Spherical Harmonics and Generalized Q-Sampling Imaging

Sudhir K Pathak[1], Catherine Fissell[2], Deepa Krishnaswamy[1], Sowmya Aggarwal[1], Rebecca Hachey[2], and Walter Schneider[2]
[1]*Bioengineering, University Of Pittsburgh, Pittsburgh, PA, United States,* [2]*Psychology, University Of Pittsburgh, Pittsburgh, PA, United States*

Introduction

Advanced diffusion reconstruction algorithms can be used to probe the complex micro-structure of white matter tissue in the human brain. One of the popular methods to resolve fiber crossings is constrained spherical deconvolution[4] (CSD) which can be used for single shell (constant b-value) image acquisitions. Generalized Q-sampling Imaging[1] (GQI) is used for Diffusion Spectrum Imaging[3] (DSI) and Multi-shell image acquisitions. We propose a new reconstruction method that combines CSD and GQI to estimate spherical harmonics (SH) coefficients for fiber Oriented Distribution Function (fODF). This method enables the advantages of CSD reconstruction[4] to be applied to DSI and multi-shell acquistions.

GQI reconstructs the diffusion oriented distribution function (dODF) from diffusion weighted images using the following equation:

$$\psi_{voxel}(\hat{u}(\theta,\varphi)) = L_\Delta \int_{\mathbb{R}^3} E_{voxel}(\vec{q}) sinc(2\,\pi\, L_\Delta\, \vec{q}\cdot\hat{u})\, d\vec{q}$$

By definition dODFs are functions defined on a unit sphere and can be represented as a linear sum of spherical harmonics[2].

$$\psi_{voxel}\big(\hat{u}(\theta,\varphi)\big) = \sum_{l=0}^{L_{max}} \sum_{m=-l}^{l} c_{lm} Y_l^m(\theta,\varphi)$$

Combining the equations above will provide an analytical expression for spherical harmonics coefficients.

$$c_j = \int_{\mathbb{R}^3} \Big(\int_\Omega L_\Delta\, sinc(2\,\pi\, L_\Delta\, \vec{q}\cdot\hat{u})\, Y_j(\theta,\varphi)\; d\Omega \Big) E_{voxel}(\vec{q})\, d\vec{q}\;\;, j = j(l.m) = \frac{l^2+l+2}{2} + m$$

To find coefficients c_j, we used the least squares method with regularization (Laplace-Beltrami operator).

Method

A 62-year-old female subject was scanned using a 3T MRI system (TIM Trio, Siemens, Erlangen, Germany) with a 32-channel coil, using a DSI protocol[3]. The field of view was 240 mm x 240 mm, matrix size 96 x 96, slice thickness 2.4mm (no gap) with 50 slices. The number of gradient directions used for DSI was 257, maximum b-value=7000 sec/mm^2, and TR / TE = 9916 ms / 157 ms. Above algorithm is implemented in MALAB to reconstruct the dODF and (fODF). Multi-FACT fiber tracking[5] was performed using DSI-Studio.

Results

The proposed reconstruction algorithm produced dODFs that have the expected advantages (over GQI) of using CSD techniques, e.g. sharper peaks and less noise (Fig1A). Tractography using fODFs produced with the proposed method yielded anatomically correct fiber tracts. In comparison to tractography using the GQI reconstruction, these tracts are more precise (note inter-hemispheric distinction in fig 1C, 1 & 2 clearly shows left and right Fornix separation). The proposed reconstruction method has the advantage that the SH parameterization of the diffusion data can be used to interpolate dODF data at subvoxel locations. There are a number of potential applications for interpolated dODFs including the high resolution estimates of diffusion direction to visualize subcortical nuclei (see 3 and 4 in fig 1D, thalamic nuclei identification only in hyper-resolution sampling) and improved tractography to visualize detailed connectivity.

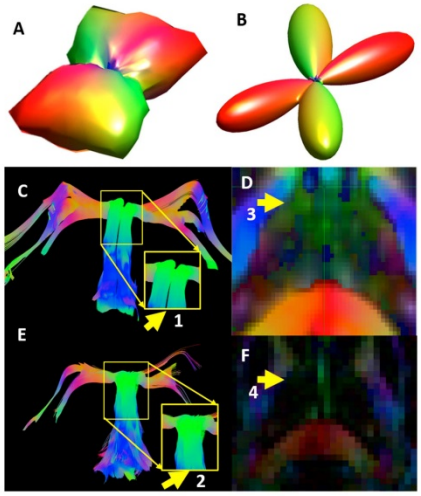

Figure 1A) dODF using GQI B) fODF using proposed reconstruction method C) Fornix track reconstructed using proposed reconstruction algorithm D) Color encoded thalamus regions showing thalamic nucleus, hype-resolution interpolation E) Fornix track reconstructed using GQI F) Color encoded thalamus regions showing thalamic nucleus, lower-resolution using GQI

Conclusion

The novel diffusion MRI reconstruction algorithm presented here is derived from current CSD and GQI methods, produces improved estimates of diffusion direction, and enables CSD techniques to be applied to DSI and multi-shell data.

References

[1] Yeh et al. 2010. [2] Maxime et al 2007. [3] Wedeen 2005. [4] Tournier et al. 2004, 2007 [5] Yeh et al 2013

PET Imaging with Pittsburgh Compound B of Amyloid Deposition in White Matter in Chronic TBI: An Exploratory Analysis

Nora Presson, Davneet S. Minhas, James M. Mountz, Catherine Fissell, Rebecca Hachey, Charles M. Laymon, Julie C. Price, Walter Schneider, David O. Okonkwo

Background. Chronic Traumatic Encephalopathy (CTE) is a neurodegenerative disorder linked to repetitive TBI. At present, CTE is an autopsy diagnosis. The goal of the current study was an exploratory analysis of whether PET imaging with Pittsburgh Compound B (PiB) can identify signs of amyloid pathology in chronic survivors of TBI.

Method. [11C]PiB PET data were acquired for 8 individuals with TBI (8 males, mean age = 47) and compared with a convenience sample of 15 healthy adults (7 males, mean age = 59). PiB SUVR images were calculated over 50-70 minutes post-injection with cerebellar grey matter (GM) as reference. Diffusion spectrum imaging data were acquired and processed in a High Definition Fiber Tracking (HDFT) pipeline. PiB SUVR data were aligned to diffusion data by registering to T1-weighted structural MR sequences as a reference. Cortical segmentation was performed on structural MRs using Freesurfer, and labels were transferred to diffusion space using the linear transformation computed with FSL software.

We used hierarchical regression to test two hypotheses in corpus callosum (CC) and cerebral WM: 1) PiB uptake differs between TBI and controls, and 2) in TBI, WM PiB uptake is correlated with diffusion anisotropy (gFA). We focused the analysis on the CC, a selectively vulnerable region in TBI.

A hierarchical model analyzed regional CC PiB SUVR treating TBI status (TBI/Control), subject age (scaled), and Freesurfer region (5 segments of CC and whole-brain cerebral WM as reference) and their 2-way interactions as fixed effects. The second hierarchical model analyzed voxel-level WM PiB SUVR using diffusion data within TBI subjects, treating gFA, Freesurfer region, and their interaction as fixed effects.

Results. Only one participant was classified as PiB-positive (elevated uptake in gray matter regions of interest for Alzheimer's Disease). Comparing control and TBI PET data, PiB SUVR was reduced in TBI subjects in Anterior and Mid-Anterior CC regions (p=.03 & p<.01). Within subjects in the TBI group, combining PET and diffusion data showed that higher gFA significantly predicted higher PiB SUVR at a voxel level in 3 of 5 CC regions and in cerebral WM (all p<.01). PiB SUVR within TBI subjects was greatest in Anterior and Mid-Anterior regions of corpus callosum (ß(anterior)=0.45, ß(mid-anterior)=0.32).

Conclusion. Pathophysiologic deposition of amyloid in white matter has been seen in experimental TBI and in autopsy series of human TBI. Our preliminary analysis found changes in PiB uptake on PET imaging in chronic TBI in the corpus callosum, a known area of vulnerability to TBI damage. This pattern is present in the absence of the typical gray matter PiB deposition seen in Alzheimer's Disease. These are promising pilot results in the search for an *in vivo* neuroimaging biomarker for CTE.

Neuropsychological Test Scores Consistently Relate to Quantitative MR Diffusion Imaging Metrics in High B-Value Multishell Imaging

Nora Presson, Sue Beers, Lisa Morrow, William Bird, Gina Droeder, Lauren Wagener, Joshua Penderville, Steven Benso, Ava Puccio, Anthony Kontos, David Okonkwo, Walter Schneider

Objective: White matter injury is hypothesized to underlie cognitive consequences of TBI. The current study correlated neuropsychological test performance with spatial properties of high bvalue advanced diffusion tractography in chronic TBI and healthy control subjects and a small acute TBI sample.

Method: Multishell, high b-value (max b = 7000) magnetic resonance (MR) diffusion imaging data were acquired and processed for white matter tractography in a High Definition Fiber Tracking (HDFT) pipeline. All participants in both chronic TBI (N = 22 injured >3mo. Before enrollment, 18 male, mean age = 38) and healthy control (N = 15, 8 male, mean age = 31) groups, as well as a small sample of individuals with acute TBI (N = 6, 5 male, mean age = 36) completed a neuropsychological test battery including Trail Making Test, California Verbal Learning Test (CVLT), WAIS-IV Processing Speed Index (PSI), Automated Neuropsychological Assessment Metrics (ANAM), and Controlled Oral Word Association Test (COWAT), as well as self-report metrics including Neurobehavioral Symptom Inventory and Behavioral Symptom Inventory (BSI-18).

Results: In the chronic TBI group, HDFT metrics of symmetry (left-right homologue correlation, in X/Y/Z dimensions) and spread (proportion of voxels contacted in left and right hemispheres) were significantly correlated with neuropsychological tests across a range of cognitive functions.
Correcting all tests for False Discovery Rate, within the TBI sample, verbal recall (CVLT) was positively correlated with Arcuate asymmetry, (Y dimension $r = 0.53$, $p = 0.01$) and Genu spread, (right hemisphere $r = 0.64$, $p < 0.01$), among others. PSI was correlated with Corona Radiata asymmetry (Y dimension $r = 0.61$, $p < 0.01$) and Genu spread (left hemisphere $r = 0.51$, $p = 0.04$), among others. Trails A was positively correlated with Cingulum asymmetry (Y dimension $r = 0.48$, $p = 0.03$) and FOF spread (right hemisphere $r = 0.57$, $p = 0.01$), among others. Trails B was positively correlated with Corona Radiata asymmetry (Y dimension $r = 0.65$, $p < 0.01$) and Uncinate spread (left hemisphere $r = 0.52$, $p = 0.01$), among others. In contrast, almost all correlations in the control sample were zero or negative. Additional exploratory analyses are discussed, including canonical correlation to combine multiple diffusion and neuropsych metrics, as well as calculating global tract severity score metrics based on the number of tracts that are outliers relative to the control (z-score < -2.32) and the summed z-score of those outlying tracts.

Conclusions: These results provide preliminary evidence that spatial white matter properties measured with tractography in high b-value MR diffusion imaging may be more informative in capturing impairment in behavioral performance following TBI than in capturing normal variability. Quantitative analysis of HDFT diffusion imaging shows promise as a biomarker of behavioral TBI outcomes.

The Effects of Adolescent Cannabis Use on Adult Working Memory

Brenden Tervo-Clemmens[1,2,3], Daniel Simmonds[1,3], and Beatriz Luna[1,2,3,4]

[1]Laboratory of Neurocognitive Development, [2]Psychology, [3]Center for the Neural Basis of Cognition,[4]Psychiatry, University of Pittsburgh

Cannabis has been associated with impairments in working memory (WM), which continues to improve through adolescence. As such, adolescents may be particularly vulnerable to the effects of cannabis on WM. However, the effect of age of onset of cannabis use on brain function supporting specific components of visuospatial working memory is not well understood. During fMRI acquisition, 54 adults with a history of cannabis use completed a Sternberg-type visuospatial working memory task where set size and maintenance duration were manipulated. For behavior analyses, we used linear-mixed-effects modeling to examine interactions between age of onset of cannabis use and the two task factors: set-size (1 or 3 locations), delay length (1.5 or 6s). A fast event-related design was used to distinguish fMRI activation encoding, maintenance, and response epochs. Only correct trials were included in group analysis. Controlling for total use, there was a negative relationship between cannabis age of onset and reaction time, which was largest in short delay trials. Age of onset was further associated with an increase in cerebellum, SMA, and bilateral mfg activation. Left mfg recruitment significantly mediated the relationship between age of onset and reaction time in short delay trials. The present findings highlight a potential pathway through which early cannabis exposure in adolescence may impair adult working memory.

Impact of Endovaginal Ultrasound on the Anatomical Positioning of Pelvic Floor Organs

Authors: Deanna C. Easley[1], Ghazaleh Rostaminia[2], Prahlad G. Menon[1], S. Abbas Shobeiri[2], Steven D. Abramowitch[1]

Affiliations: University of Pittsburgh[1], University of Oklahoma[2]

Background

MRI is the gold standard for diagnosing pelvic floor disorders, and is often paired with various measurement techniques to determine the position of pelvic organs and quantify defects. However, ultrasound is gaining popularity due to its many advantages, including: affordability, wide availability, and reduced scan time.

Significance

The endovaginal probe provides optimal visualization of the pelvic floor; however, it also distorts the contours of the vagina. Therefore, given its affordability and availability, it is important to ascertain whether ultrasound can be a reliable method for determining anatomical position relative to MRI.

Methods

Four subjects were selected based on the availability of same-day 3D endovaginal ultrasounds and MRIs. The urethra, rectum, pubic rami, and levator ani muscles were segmented using Seg3D. Different observers segmented ultrasound and MRI volumes independently. Ultrasound scans and corresponding segmentations were manually aligned to match bony contours using Seg3D and Slicer software. Isosurfaces were generated from these segmentations, and voxel smoothing was finalized using 3DCoat. An iterative closest point algorithm was utilized to shift ultrasound isosurfaces onto those generated from MRI and measure the distance between segmented organs.

Results

Ultrasound volumes noted a measurable anterior shift of the urethra and a posterior shift of the rectum by the probe. The urethra and rectum showed maximum mean shifts of 4.2 mm (s.d. 3.3) and 6.1 mm (s.d. 3.7), respectively.

Conclusions

The ultrasound probe does distort the pelvic organs, however, the distortion is minimal, indicating that neutral insertion of the probe likely provides comparable spatial measurements to MRI.

Perfluorocarbon Nanoemulsions for High Intensity Focused Ultrasound Induced Anticancer Drug Delivery – In vitro study

Eric Lambert[1], Jelena M. Janjic*[1,2]

[1] Graduate School of Pharmaceutical Sciences, Duquesne University, Pittsburgh, Pennsylvania, United States;
[2] McGowan Research Institute for Regenerative Medicine, Pittsburgh, Pennsylvania, United States

Cancer progression is naturally accompanied by inflammation. Clinical studies have demonstrated that tumor-associated inflammation promotes metastasis, increases tumor resistance to chemotherapy and overall decreases patient survival. Anti-inflammatory drugs (e.g. NSAIDs) were investigated as anti-cancer therapeutics with mixed results. We propose that tumor associated inflammation, specifically macrophages, can be therapeutically targeted by anti-cancer drug loaded nanoemulsions. Further, their effectiveness can be dramatically increased by applying magnetic resonance-guided high intensity focused ultrasound (HIFU) as the means of maximizing drug payload release in tumors. Previously we have shown that triphasic perfluorocarbon (PFC) nanoemulsions can selectively target macrophages in live animals (Patel, Beano et al, Clinical Immunology 2015). We propose here that these triphasic, perfluorocarbon nanoemulsions can target the tumor infiltrating macrophages, and, under exposure to HIFU, deliver their therapeutic payload specifically to tumors. Here we report a formulation and assessment strategies towards HIFU using triphasic PFC/hydrocarbon (HC) nanoemulsions. Specifically we evaluated the effects of different PFC:HC ratios and structural effects of PFC on nanoemulsions colloidal behavior. All nanoemulsions were manufactured by microfluidization using earlier reported methods. Colloidal stability test results including serum stability and long term size and zeta potential will be presented.